The experimental data indicated a larger dependence than theoretically suggested.

The comparison of the best-fit power law curve of these data points with the shape of the rms wave slope–wind speed dependence resulting from optical observations and from the microwave specular-point scattering model indicates that the *S*-band brightness temperature increase is dominated by wave slope distribution (local wind fields) rather than by significant wave height.

Acknowledgment

The authors wish to thank R. N. Parker, J. E. Stitt both of NASA Langley Research Center and J. Lehmann, NASA Headquarters, for their support of this project under the AAFE program. We express our appreciation to the Wallops Flight Center staff for their valuable assistance and aircraft support, and to Johns Hopkins University for supplying the Chesapeake Bay ground-truth data. We also wish to thank C. Cox formerly with LTV Aerospace Corporation and E. C. Hooper NASA Langley Research Center for their fine work in the installation and calibration of the system, and for the help in taking these data.

References

[1] W. L. Smith, P. K. Rao, R. Koffler, and W. R. Curtis, "Determination of sea surface temperature from satellite Hi-resolution infrared window radiation measurement," *Monthly Weather Review*, vol. 98, pp. 604–611, 1971.
[2] J. L. Cogan and J. H. Willare, "Measurement of sea surface temperature by the NOAA-2 satellite," in *Third Symposium on Meteorological Observations and Instrumentation*, Feb. 10, 1975, pp. 123–130.
[3] E. D. McAlister and W. McLeish, "Heat transfer in the top millimeter of the ocean," *J. Geophys. Res.*, vol. 74, pp. 3408–3414, 1969.
[4] W. N. Hardy, K. W. Gray, and A. W. Love, "*S*-band radiometer design for high absolute precision measurements," *IEEE Trans. Microwave Theory and Tech.*, vol. MTT-22, no. 4, pp. 382–390, April 1974.
[5] W. W. Ho and W F. Hall, "Measurements of the dielectric properties of sea water and NaCl solutions at 2.65 GHz," *J. Geophys. Res.*, vol. 78, p. 6301, 1973.
[6] W. W. Ho, A. W. Love, and M. J. Van Melle, "Measurements of the dielectric properties of sea water at 1.43 GHz," NASA CR-2458, National Technical Information Service, Springfield, VA 22151, Dec. 1974.
[7] E. H. Grant, T. J. Buchanan, and H. F. Cook, "Dielectric behavior of water at microwave frequencies," *T. Chem. Physics*, vol. 26, no. 1, p. 156, Jan. 1957.
[8] *Reference Data for Radio Engineers.* New York: Howard W. Sams and Co., Inc., 1968.
[9] J. R. Shakeshaft and A. S. Webster, "Microwave background in steady state universe," *Nature*, vol. 217, p. 339, 1968.
[10] G. M. Hidy *et al.*, "Development of a satellite microwave radiometer to sense the surface temperature of the World's oceans," NASA Final Rep. CR-1960, National Technical Information Service, Springfield, VA 22151, 1972.
[11] W. W. Ho *et al.*, "Brightness temperature of the terrestrial sky at 2.66 GHz," *J. Atm. Sci.*, vol. 29, p. 1210, 1972.
[12] F. B. Beck, "Antenna pattern corrections to microwave radiometer temperature calculations," *Radio Science*, vol. 10, pp. 839–845, Oct. 1975.
[13] W. N. Hardy, "Precision temperature reference for microwave radiometer," *IEEE Trans. Microwave Theory and Tech.*, vol. MTT-21, no. 3, pp. 149–150, March 1973.
[14] R. J. Wagner and P. J. Lynch, "Analytical study of microwave sea brightness temperature: A composite surface model," ONR, Dept. of Navy Final Report, Contract N00014-71-C-0240, 1972.
[15] J. P. Hollinger, "Passive microwave measurements of sea surface roughness," *IEEE Trans. Geosci. Electron.*, vol. GE-9, p. 166, 1971.
[16] C. T. Swift, "Microwave radiometer measurements of the Cape Cod Canal," *Radio Science*, vol. 9, no. 7, pp. 641–653, July 1974.
[17] C. Cox and W. Munk, "Measurement of the roughness of the sea surface from photographs of the Sun's glitter," *J. of the Optical Soc. of Am.*, vol. 44, no. 11, pp. 838–850, Nov. 1954.
[18] D. E. Barrick, "Wind dependence of quasi-specular microwave sea scatter," *IEEE Trans. Antennas and Propagat.*, vol. AP-22, no. 1, pp. 135–136, Jan. 1974.

Succinct Papers

High-Resolution Mapping of Oceanic Wind Fields with Skywave Radar

JAMES R. BARNUM, MEMBER, IEEE,
JOSEPH W. MARESCA, JR., AND SIDNEY M. SEREBRENY

***Abstract*—The direction of the mean surface wind field in the North Pacific Ocean was mapped on September 25 and 26, 1973, over an area of 3 × 10^6 (km)^2 by OTH-B HF radar. A spatial resolution of 60 km in range and 15 km in cross range was used at points spaced by 150 km in range and 80 km in cross range. Wind directions were inferred from the upwind/downwind first-order Bragg ratio and the measure of the maximum ratio occurring for radial winds at points near each observation. Over 90 percent of the recorded data were usable for this purpose. High spatial resolution is essential to make detailed measurements of the wind speed and direction across and along an atmospheric cold front. The location of the atmospheric cold front derived from the wind field agreed well with the ESSA VIII satellite frontal location.**

Manuscript received October 2, 1975; revised April 16, 1976. This work was supported in part by the Office of Naval Research and the National Science Foundation as part of the North Pacific Experiment (NORPAX).
The authors are with the Remote Measurements Laboratory, Stanford Research Institute, Menlo Park, CA 94025.

I. Introduction

Measurements of ocean surface winds are important to the understanding of air/sea interaction. Along with desert and polar areas, the oceans comprise vast data-sparse regions. The violent and destructive tropical cyclones are spawned and grow to great dimensions and intensities in such areas. On these occasions, ocean surface measurements are especially desirable.

Inferences of ocean surface waves and winds have been achieved remotely with the use of high-frequency (HF) skywave radar. Very long ranges are made possible when the ionosphere

is used to return the radar signals to earth [1]. Long and Trizna [2] were first to publish skywave radar maps of ocean wind direction using an empirical technique relating the wind direction to the first-order Bragg scatter ratio from approaching and receding waves. Ahearn *et al.* [3] mapped ocean wind directions with the method in [2], and also attempted to infer ocean wind speeds from the ocean scatter magnitude near zero Doppler. Stewart and Barnum [4] developed a method for inferring wind velocity at long ranges by skywave radar. Wind direction was inferred from the first-order Bragg scatter ratio from approaching and receding waves, using a model for the ocean wave directional spectrum that is a function both of wind speed and radio frequency. The wind speed was inferred from the Doppler spectrum width centered on the strongest Bragg return at a level 10 dB lower than the Bragg peak. Maresca and Barnum [5] have improved this measure of wind speed by accounting for the effect of radar frequency and have discussed the theoretical limitations. Reliable measures of ocean surface winds accompanied the data discussed in [4] and [5], from which we now deduce accuracies of $\pm 16°$ in wind direction and ± 2.4 m/s in wind speed within one standard deviation relative to the measures *in situ*.

Skywave radar coverage far exceeds that of HF surface wave, but two potential problems exist with the use of ionospheric propagation for the purpose of sea scatter analysis: 1) a coherence time limit caused presumably by the motion of fine-scale irregularities; and 2) the simultaneous reception of more than two propagating modes (multipath) from different areas of the sea. The coherence time allowed by the ionosphere will generally limit the Doppler resolution to between 0.1 and 0.01 Hz [5], [6] at middle latitudes, and can be expected to be poorer at more northerly latitudes [6]. The highest coherence is found for *E*-layer reflection, because it affords the least penetration of the ionosphere. Unfortunately, this low layer prohibits propagation beyond about 2000 km range via a single hop, and it is effectively absent between sunset and sunrise. Multipath propagation is evident in a large percentage of data recorded [5] and is considerably more prevalent at ranges exceeding 3000 km via single-hop *F*-layer propagation [4]. Multipath will always obscure some portion of the sea scatter Doppler spectrum, when viewed as a whole, but will usually not affect the measure of wind direction and will not always limit inference of wind speed from the scatter located near the two first-order Bragg returns [5].

This paper illustrates the results of a two-day skywave radar scatter experiment over the Pacific Ocean. The direction of the ocean wind field was mapped to high resolution over 3×10^6 $(\text{km})^2$ and the wind velocity was detailed across a cold front. It will be shown that significant changes in wind direction occur over space scales on the order of 20 km or less, such that high radar resolution was indispensible. Ionospheric effects on these data are discussed.

II. Theory

The method for determination of wind speed from the second-order scatter contribution to the Doppler spectra has been discussed elsewhere [4], [5]. To infer the wind direction we assumed that the 2- to 3-s waves responded within a short time to the local winds, and that the mean direction of these waves represents the mean wind direction over the same period of time. The determination of wind direction for the September 1973 experiment is analogous to that of Long and Trizna [2]. The sea-wave energy directional spectrum $F(\theta)$, for $|\theta| \leq \pi/2$, was assumed to be somewhere between semi-isotropic and cosine squared:

$$F(\theta) = A + B\cos^2\theta \tag{1}$$

where A and B are arbitrary constants, and θ is the angle between the wind and wave directions. It was also found empirically [2] that

$$F(\pi - \theta) = \frac{F^2(\pi/2)}{F(\theta)}. \tag{2}$$

We define the ratio of first-order Bragg line amplitude in the approaching and receding directions by $X(\theta)$, where

$$X(\theta) \triangleq \frac{F(\theta)}{F(\pi - \theta)}. \tag{3}$$

Nearest each data scan we measure the maximum $X(\theta)$ at $\theta = 0$ or the inverse of the minimum X at $\theta = \pi$, with either one called X_m, and we define $X(\pi/2) = 1$. We then find that

$$X(\theta) = \begin{cases} [1 + K\cos^2\theta]^2, & 0 \leq |\theta| \leq \pi/2 \\ [1 + K\cos^2\theta]^{-2}, & \pi/2 \leq |\theta| \leq \pi \end{cases} \tag{4}$$

where

$$K = (X_m - 1)^{1/2}. \tag{5}$$

Equation (4) can be inverted to express θ as a function of X.

In [2] and [3] we find that X_m was assumed to be constant for all data recorded, regardless of the operating frequency or wind speed. In light of the work by Tyler *et al.* [7], we cannot hold X_m constant for our experiment. By assuming constant X_m we fix the sea wave directional spectrum for all time. Tyler *et al.* concluded that $F(\theta)$ is a function of both the radio frequency and wind speed, and used a different functional representation for $F(\theta)$, which is a modification of the form suggested by Longuet-Higgins *et al.* [8]. When we constrain the $F(\theta)$ in [7] to match observed values of X_m with $X(\pi/2) = 1$, we calculate a maximum of only 11° difference between θ predicted, using $F(\theta)$, by both methods. We have used the measured X_m nearest to each recorded spectra, thereby updating (4) with (5) for all data reported herein. X_m varied between 14 and 24 dB, with a mean of 21 dB. We believe that any effects on $F(\theta)$ caused by changes in radio frequency and wind speed have thus been partially accounted for.

III. Radar Data Processing

The reader is referred to a paper by Skolnik and Headrick [9] for an introduction to OTH radar practices, and to a paper by Croft [1] for illustrations of data recorded via skywave propagation. The Wide Aperture Research Facility (WARF) was used to record the data. Some details regarding the WARF radar, and examples of swept-frequency ocean backscatter amplitude were published by Barnum [10]. A more recent summary was published in report form by Marshall and Barnum [11]. The WARF coverage is shown in Fig. 1.

Briefly, WARF is a bistatic system with 185 km separation between transmitter and receiver in central California. This large-receiving-aperture (2.55 km) radar yields a radar antenna beamwidth of $\frac{1}{3}°$ at 20 MHz. A time-delay resolution of 20 μs was used to record our data (where 1 μs is close to 150 m of ground range for this skywave experiment). Thus, we processed ocean areas with dimensions of 15 km (average) in cross range and 3 km in range. A total of 21 of these cells were averaged

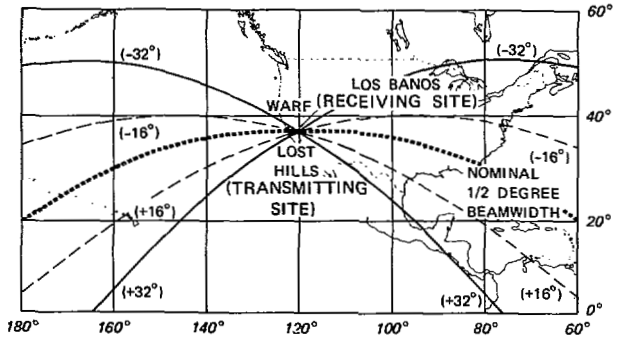

Fig. 1. WARF radar azimuth coverage to east and west of California.

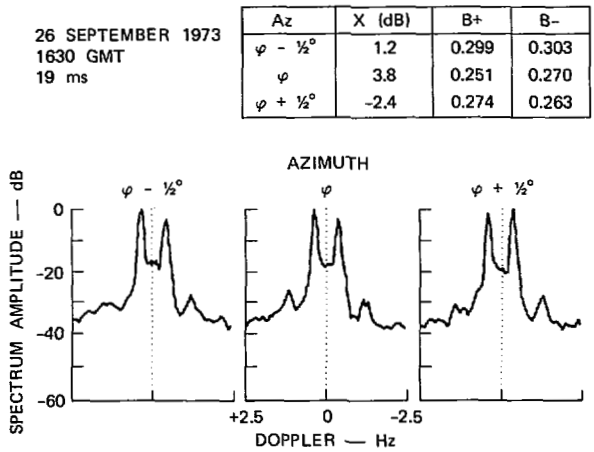

Fig. 2. Example of real-time backscatter display used for recording data for wind-field mapping. Each such display is updated once per minute at new ocean location. Center azimuth was used to map wind fields.

incoherently to smooth the scattering statistics, resulting in a net spatial average of 15 km × 63 km.

Performance assurance of the WARF radar is achieved through simultaneous operation of a low-power wide-frequency swept-backscatter system used to estimate the mode of signal propagation to the area of interest and to specify usable operating frequencies. Examples of such data were published by Croft [1] and Barnum [10].

Three-dimensional displays of backscatter amplitude versus time delay (range) and Doppler frequency are first processed by means of a Fourier transform of the radar signals. The Doppler coverage extends from +2.5 Hz to −2.5 Hz. The raw samples are weighted by a cosine-squared window to reduce frequency sidelobes. A coherent integration of 12.8 s was used exclusively with the data discussed in this paper.

Noncoherent spectrum averaging was used to smooth the statistical variation of sea scatter amplitude. Unpublished data show that the coefficient of variation of the spectrum samples in space followed a Rayleigh distribution for all noncoherent time averages. Two noncoherent time averages and 21 spatial (range-cell) averages were performed prior to each spectrum output in this experiment. This should produce a very smooth estimate of the representative scatter spectrum [5].

Fig. 2 is an example of the processor output used in this experiment. These data were updated once per minute. Three adjacent antenna beams, spaced by ½°, were sampled and processed simultaneously. A log of radar operating parameters was recorded automatically. The Bragg line ratio X, and spectrum width B were also calculated automatically for each azimuth,

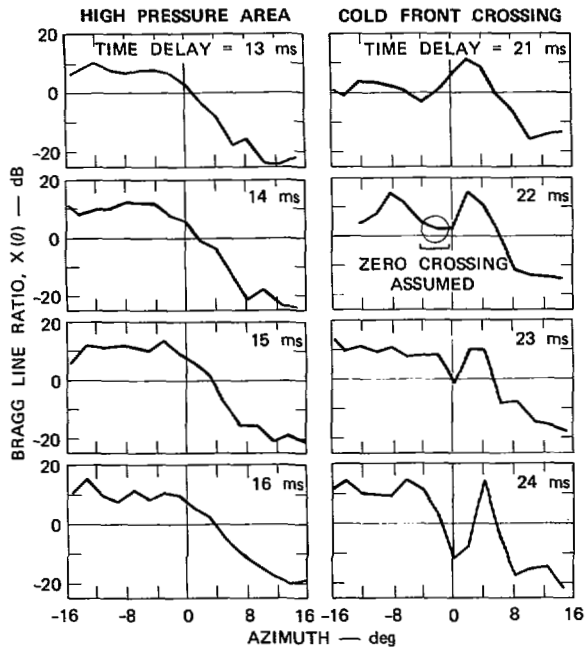

Fig. 3. Bragg-line ratio, $X(\theta)$ versus radar azimuth at eight time delays on September 26, 1973. Circulation to SW of high-pressure system was sampled by data between 13 and 16 ms, while cold front was crossed by scans between 21 and 24 ms.

and are labeled X and B, respectively, on Fig. 2. Note that X changed by 6.2 dB over an azimuth difference of only 0.5°.

IV. Data Collection and Interpretation

Data similar to Fig. 2 were recorded sequentially by stepping every 2° in azimuth at a constant radar time delay and frequency. The frequency of operation was checked prior to each scan to ensure adequate propagation along each scan. Time delays were stepped in 1-ms increments between 10 and 27 ms on the first day, and between 13 and 25 ms on the second day, using $F2$-layer propagation. The longer ranges were sampled earlier in the day because multipath was least prevalent at those times.

Propagation conditions were usually different at the two ends of an azimuth sector, such that more optimum time delays and/or frequencies could have been chosen for different portions of each scan. Ionospheric multipath often appeared over portions of a scan at azimuths where the skip distance was approached too closely. Examples of multipath are illustrated by Maresca and Barnum [5]. About 50 percent of the data revealed some form of multipath. The calculation of $X(\theta)$ for wind direction was rarely affected by multipath, but not all spectra can be reduced for wind speed using B. The data beyond 20 ms (3000 km) were the most often perturbed, which is consistent with the findings of Stewart and Barnum [4].

All spectra from the experiment were first reduced for the Bragg line ratio X, and this was plotted versus azimuth, parametric in time delay. Fig. 3 is an example of some of these plots on September 26, 1973. The plots on the left of the figure represent scans to the west of an anticyclone and to the east of a cold front. The maximum observed values of X (in absolute decibels) occurred in the trade wind region, since the winds were approximately parallel to the radar heading. The plots on the right side of the figure contain radar crossings of a weather front that noticeably interrupted the otherwise continuous nature of X versus azimuth. The weather front usually caused a double zero crossing in X that is seen at azimuths between −6°

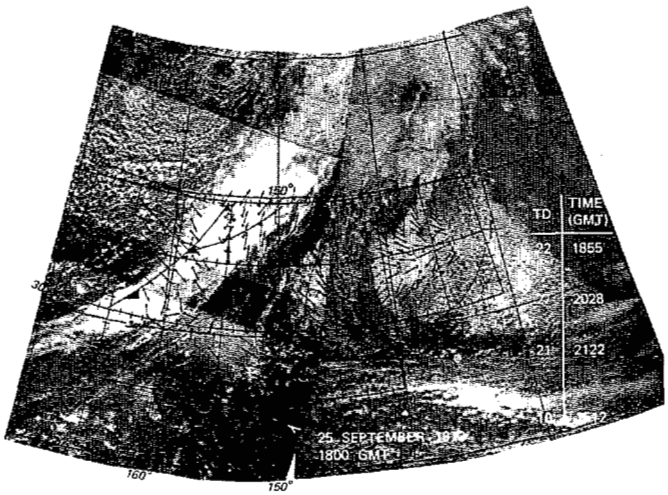

Fig. 4. Radar weather map for September 25, 1973, compared to NWS analysis of 1800 GMT and ESSA VIII cloud photograph on morning of same day. Radar winds represented are for times between 1800 and 2400 GMT. Wind direction is plotted by arrows: feet of arrows denote positions. Since NWS surface chart and radar weather maps are mercator projections and satellite photograph is not, there is some distortion in outer regions when comparing them.

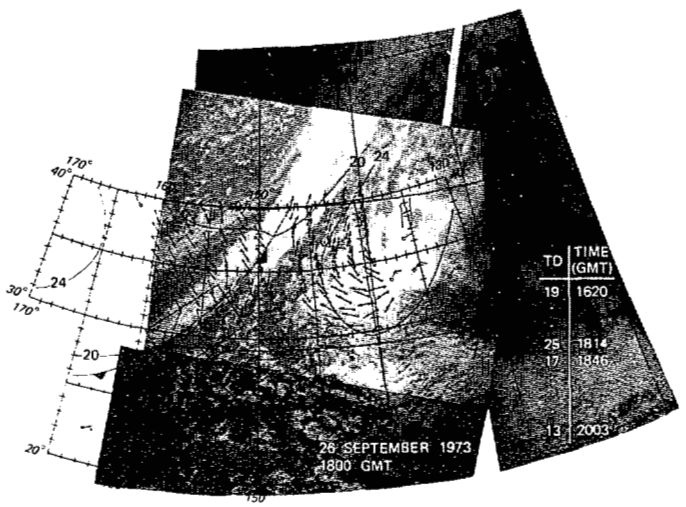

Fig. 5. Radar weather map for September 26, 1973 compared to NWS map at 1800 GMT and ESSA VIII cloud photograph (similar to Fig. 4). Radar data reflected winds blowing between hours of 1530 and 1900 GMT. Almost all of data agree well with ship-measured winds and NWS-assumed location of cold front and high-pressure center.

and 2° in Fig. 3, depending on the time delay. These zero crossings essentially accounted for net changes in wind direction exceeding 180°. Note that the minimum in X between these crossings advances in azimuth from $-4°$ at 21 ms delay, to between 0° and 2° at 24 ms delay. This trend was interrupted by a dip at $-2°$ at 22 ms with a lack of a zero crossing. Since crossings were also observed at 19 ms and 20 ms delays, a reversal of wind direction was therefore assumed to occur at $-2°$ azimuth at 22 ms.

The left/right ambiguity in θ [2], [3] was resolved by knowledge of the expected anticyclonic circulation around the high-pressure cell shown on the National Weather Service (NWS) map and cloud photograph. Each zero crossing yields a wind that is crosswise to the radar bearing, a condition that usually occurred across the cold front.

V. Radar Wind Field Maps

The radar-derived wind field for the first day, September 26, 1973, is shown in Fig. 4, and is compared with the relevant portion of the ESSA VIII cloud photograph and NWS surface analysis for 1800 GMT. The radar data were recorded between the hours of 1855 GMT and 2512 (0112) GMT. We expect the data at the lower time delays (later in the day) to disagree with the ship reports taken some 6 to 7 h earlier.

In the ESSA VIII cloud photograph the cold front is identified by a well-developed elongated bright band of clouds oriented NE/SW extending through 40°N, 150°W. The cellular-appearing clouds between 140°W and 130°W and near 30°N are characteristic of clouds around the southwestern perimeter of an oceanic high-pressure area ahead of a well developed cold front. The center of the high-pressure area is located somewhere in the clear area in the right-hand edge of the photograph.

The general agreement between the radar-derived wind fields and the independent surface-wind measurements on September 25 was good. The cold front position shown in Fig. 4 was plotted by NWS approximately 200 nmi to the northwest of the front indicated by the radar data. The radar-inferred wind shifts agree with the wind shifts implied by the satellite cloud photograph displaying and locating the frontal cloud cover. The discontinuous nature of the wave field recorded by the radar is a good method for detailing the position of the front and the wind field across the front.

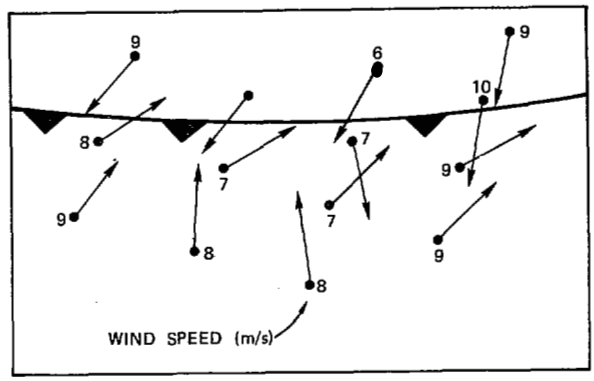

Fig. 6. Wind speed, in meters per second, and direction arrows in vicinity of atmospheric front on September 26, 1973.

The radar-derived wind field for the second day, September 26, 1973, is shown in Fig. 5, and is compared with the ESSA VIII cloud photograph and NWS analysis for 1800 GMT. The radar data on the second day were recorded between the hours of 1620 GMT and 2003 GMT. The radar winds again showed the frontal wind discontinuity very clearly, as well as a wind discontinuity associated wtih a trough in the easterlies west of 155°W and proximal to 25°N.

The magnitude of the wind was added to 13 out of the 14 direction vectors in the area outlined on Fig. 5 in the vicinity of the cold front. The method described by Stewart and Barnum [4], with the improvements illustrated by Maresca and Barnum [5], was used. The results are illustrated in Fig. 6.

VI. Conclusions

The most important contribution found in this experiment was the ability to use long range skywave radar to detect the abrupt wind shifts across the cold front. Thus, when rapid spatial variations in wind fields occur, the high-frequency sea waves will also respond rapidly and this response can be detected by the radio wave backscatter. High spatial resolution was thus essential for the detection of these abrupt wind direction changes. In

Fig. 2, for example, a 16° direction shift occurred over only $\frac{1}{2}$° of radar azimuth, equivalent to about 15 km in cross range. Range resolutions of comparable size are essential to the analysis of atmospheric fronts and the gradient of wind stress across intense cyclones. Resolutions of 3 km are readily achievable with the WARF radar.

Ionospheric conditions varied both in space and time. These variations were not abnormal. Multipath was most severe at ranges exceeding 3000 km. This limitation was reduced by recording data at the longer ranges earlier in the day. Over 90 percent of high-resolution sea backscatter Doppler spectra recorded on these two successive days over an area exceeding 3×10^6 (km)^2 were readily usable for calculation of the mean oceanic wind direction. Due to ionospheric perturbation of the echoes, a lesser number could be used for calculation of wind speed. It is clear that the percentage of data usable for wind speed can be increased by matching radar parameters to ionospheric skip parameters at each observation point. For example, a north–south azimuth scan at a constant radio frequency should incorporate a variable time-delay (range) gate to match north–south tilts in ionospheric electron density.

References

[1] T. A. Croft, "Sky-wave backscatter: A means for observing our environment at great distances," *Rev. Geophys. Space Phys.*, vol. 10, pp. 73–155, Feb. 1972.

[2] A. E. Long and D. B. Trizna, "Mapping of North Atlantic winds by HF radar sea backscatter interpretation," *IEEE Trans. Antennas Propagat.*, vol. AP-21, pp. 680–685, Sept. 1973.

[3] J. L. Ahearn, S. R. Curley, J. M. Headrick, and D. B. Trizna, "Tests of remote skywave measurement of ocean surface conditions," *Proc. IEEE*, vol. 62, pp. 681–687, June 1974.

[4] R. H. Stewart and J. R. Barnum, "Radio measurements of oceanic winds at long ranges: An evaluation," *Radio Science*, vol. 10, pp. 853–857, Oct. 1975.

[5] J. W. Maresca, Jr., and J. R. Barnum, "Measurement of oceanic wind speed from HF sea scatter by skywave radar," *IEEE Trans. Antennas Propag.*, this issue, pp. 132–136.

[6] R. A. Shepherd and J. B. Lomax, "Frequency spread in ionospheric radio propagation," *IEEE Trans. Commun. Technol.*, vol. COM-15, pp. 268–275, April 1967.

[7] G. L. Tyler *et al.*, "Wave directional spectra from synthetic aperture observations of radio scatter," *Deep-Sea Research*, vol. 21, pp. 989–1016, 1974.

[8] M. S. Longuet-Higgins, D. E. Cartwright, and N. D. Smith, "Observations of the directional spectrum of sea waves using motions of a floating buoy," *Ocean Wave Spectra*. Englewood Cliffs, NJ: Prentice-Hall, 1963, pp. 111–136.

[9] J. M. Headrick and M. I. Skolnik, "Over-the-horizon radar in the HF band," *Proc. IEEE*, vol. 62, pp. 664–673, June 1974.

[10] J. R. Barnum, "Skywave polarization rotation in swept-frequency sea backscatter," *Radio Science*, vol. 8, pp. 411–423, May 1973.

[11] W. F. Marshall and J. R. Barnum, "Measurement of sea scatter and buoy tracks at long ranges by high-resolution OTH-B radar," Technical Report 1 (NR 083-320), Stanford Research Institute, Menlo Park, CA, May 1975.

Measurement of Oceanic Wind Speed from HF Sea Scatter by Skywave Radar

JOSEPH W. MARESCA, JR., AND JAMES R. BARNUM,
MEMBER, IEEE

Abstract—**Remote measurements of the spatial mean ocean wind speeds were obtained using Doppler spectra resolved to 0.08 Hz from high-resolution HF skywave-radar backscatter measurements of the ocean surface. A standard deviation of 2.4 m/s resulted from the correlation of observed winds over the ocean and the broadening of the Doppler spectra in the vicinity of the higher first-order Bragg line. This broadening, for Doppler spectra unperturbed by the ionospheric propagation, is proportional to the increase in power caused by higher order hydrodynamic and electromagnetic effects in the vicinity of the Bragg line and inversely proportional to the square root of the radio frequency. A lower bound on the measure of wind speed was established at 5 m/s by the low resolution spectral processing and low second-order power. An upper limit is suggested by the steep slope in the region of the sea backscatter spectrum outside the square root of two times the first-order Bragg line Doppler.**

Manuscript received October 2, 1975; revised April 16, 1976. This work was supported in part by the Office of Naval Research and the National Science Foundation as part of the North Pacific Experiment (NORPAX).

The authors are with the Remote Measurements Laboratory, Stanford Research Institute, Menlo Park, CA 94025.

I. Introduction

High-resolution HF skywave radar measurement of ocean surface winds over large areas of ocean are important to the study of large-scale air/sea energy exchanges. Empirical estimates of the ocean surface wind are an indirect measurement based on the ocean wave field which acts as a scattering surface. Theoretical models of the hydrodynamic and electromagnetic contributions to the backscatter Doppler spectrum and their comparison with data obtained from HF surface-wave radar have been published by Barrick [1] and Johnstone [2]. The surface roughness is represented by an assumed form of the ocean wave spectrum. If the assumed functional form of the wave spectrum results in a good fit between the model of the Doppler spectrum and the measured Doppler spectrum, then sea state is predictable. For fully developed conditions, the match between the theory and the measured return is good. Using the second-order power theory, Johnstone correlated wind speed with the ratio of the second-order power to the first-order power. Simpler determinations of wind speed from empirical correlations based on the second-order theory have been developed by Ahearn *et al.* [3] and Stewart and Barnum [4]. Ahearn *et al.* correlated the increase in power measured at the lowest level between the Bragg lines with the wind speed, and Stewart and Barnum correlated the increase in the -10 dB spectral width of the Doppler spectrum, defined as B, in the vicinity of the higher Bragg line.

The objectives of this paper are to report an improvement in the correlation of B with wind speed, originally presented by Stewart and Barnum, by accounting for a difference in radar operating frequencies, and to discuss the accuracy of the technique.

II. Theoretical Considerations and Data Normalization

The wind speed obtained from the spectral broadening in the vicinity of the stronger Bragg line is a spatial average of the mean wind required to generate the waves in a given area of ocean at the time of the radar backscatter measurement; it is not a measure of the instantaneous wind. B is a measure of this spectral broadening on data processed with 12.8 s of coherent integration with cosine-squared weighting on the received waveform. It was defined [4] as the width of the Doppler spectrum 10 dB down from the maximum Bragg line power. At this spectral resolution (0.078 Hz), the higher order contributions are separate (Fig. 1(a)), but not uniquely resolvable from the Bragg-line power (Fig. 1(b)). The spectral broadening in this region has been shown [1], [2] to be a function of the higher order electromagnetic and hydromagnetic effects of scattering from the ocean surface. It is probable that the increase in second-order power in the Doppler spectrum is a result of the low-frequency portion of the wave spectrum. This is suggested by a comparison of the second-order power obtained from the form of the ocean wave spectrum suggested by Phillips [5], which has a vertical low-frequency cutoff that eliminates the energy contribution at the lower frequencies, with the form of the ocean wave spectrum